

# Substituted Metal Carbonyls. 26.<sup>1</sup> One-Step Synthesis, Structures, NMR, and Dynamic Laser-Light Scattering of $\text{Re}_2(\mu\text{-OMe})_2[\mu\text{-Ph}_2\text{P}(\text{CH}_2)_n\text{PPh}_2](\text{CO})_6$ ( $n = 1\text{--}4$ )

Pauline M. N. Low, Yuk Lin Yong, Yaw Kai Yan,<sup>†</sup> and T. S. Andy Hor\*

Department of Chemistry, Faculty of Science, National University of Singapore, Kent Ridge 119260, Singapore

Sik-Lok Lam, Kam Kwong Chan, Chi Wu, and Steve C. F. Au-Yeung\*

Department of Chemistry, The Chinese University of Hong Kong, Shatin, NT, Hong Kong

Yuh-Sheng Wen and Ling-Kang Liu\*

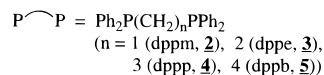
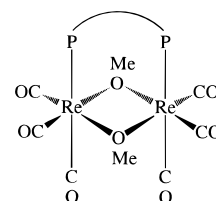
Institute of Chemistry, Academia Sinica, Taipei 11529, Taiwan

Received August 29, 1995<sup>⊗</sup>

Oxidative decarbonylation of  $\text{Re}_2(\text{CO})_{10}$  by  $\text{Me}_3\text{NO}$  in a mixture of THF and MeOH followed by addition of alkyl-chained diphosphine  $\text{Ph}_2\text{P}(\text{CH}_2)_n\text{PPh}_2$  (PP) ( $n = 1\text{--}4$ ) gives  $\text{Re}_2(\mu\text{-OMe})_2(\mu\text{-PP})(\text{CO})_6$  in 34, 29, 28, and 10% yields, respectively. This methanolytic oxidation across the Re–Re bond provides a general and one-step route for the synthesis of these dirhenium hexacarbonyl complexes with diphosphine and methoxo bridges. The molecular structure of  $\text{Re}_2(\mu\text{-OMe})_2(\mu\text{-Ph}_2\text{PCH}_2\text{PPh}_2)(\text{CO})_6$  was determined by single-crystal X-ray diffraction analysis. It contains two *fac*-[Re(CO)<sub>3</sub>] moieties bridged by dppm and two methoxo ligands. The {Re<sub>2</sub>O<sub>2</sub>} core is significantly more planar than that in the  $\text{Fe}(\text{C}_5\text{H}_4\text{PPh}_2)_2$  analogue. That such a dinuclear core is maintained in spite of the different steric demands of the different bridging diphosphines illustrates the great geometric tolerance of the bridging methoxo groups. The fluxionality of the dppm, dppe, and dppp complexes has been studied and compared by molecular modeling and solution <sup>1</sup>H NMR spectroscopy. Dynamic laser-light scattering (DLS) shows that the dppe complex aggregates in  $\text{CH}_2\text{Cl}_2$  to form small clusters with an average radius of ~370 nm. The use of a combination of DLS and NMR in organometallic chemistry is unprecedented.

## Introduction

Diphosphine-substituted carbonyl complexes of rhenium have attracted recent interest with regard to their reactivities and electrochemical and photochemical properties.<sup>2</sup> We recently reported the facile synthesis of the bis(methoxo) complex  $\text{Re}_2(\mu\text{-OMe})_2(\mu\text{-dppf})(\text{CO})_6$  (**1**; dppf = 1,1'-bis(diphenylphosphino)ferrocene) based on a room temperature activation of a Re–Re bond in  $\text{Re}_2(\text{CO})_{10}$  in methanol.<sup>3</sup> The analogous dppm ( $\text{Ph}_2\text{PCH}_2\text{PPh}_2$ ) complex **2** had been previously reported as a side product in the photolysis of  $\text{Re}_2(\text{CO})_8(\mu\text{-dppm})$ .<sup>4</sup> Although the [Re<sub>2</sub>(μ-OMe)<sub>2</sub>] core does not appear to have flexibility in adjusting its Re···Re separation, it surprisingly can accommodate a bridging phosphine such as dppf<sup>5</sup> or dppm,<sup>6</sup> which differ in steric and conformational demands. It is rare for bridging methoxo ligands



to support bridging diphosphines with both short and extended backbones. In order to understand this behavior, and in view of the current significance of alkoxo complexes of Re(I),<sup>7</sup> we have extended this study to other diphosphines. It is our aim to establish if this Re–Re activation mechanism can provide a general route to other methoxo carbonyl complexes and if the different chain lengths of the phosphines would necessitate any structural changes. Should a dinuclear frame

\* To whom correspondence should be addressed.

<sup>†</sup> Present address: Division of Chemistry, National Institute of Education, 1025 Singapore.

<sup>⊗</sup> Abstract published in *Advance ACS Abstracts*, February 1, 1996.

(1) Part 25 Fang, Z.-G.; Wen, Y.-S.; Wong, R. K. L.; Ng, S.-C.; Liu, L.-K.; Hor, T. S. A. *J. Cluster Sci.* **1994**, *5*, 327–340.

(2) Marchi, A.; Marvelli, L.; Rossi, R.; Magon, L.; Uccelli, L.; Bertolasi, V.; Ferretti, V.; Zanobini, F. *J. Chem. Soc., Dalton Trans.* **1993**, 1281–1286. Braunstein, P.; Douce, L.; Balegronne, F.; Grandjean, D.; Bayeul, D.; Dusausoy, Y.; Zanollo, P. *New J. Chem.* **1992**, 925.

(3) Yan, Y. K.; Chan, H. S. O.; Hor, T. S. A.; Tan, K.-L.; Liu, L.-K.; Wen, Y.-S. *J. Chem. Soc., Dalton Trans.* **1992**, 423–426.

(4) Lee, K.-W.; Pennington, W. T.; Cordes, A. W.; Brown, T. L. *Organometallics* **1984**, *3*, 404.

(5) Gan, K. S.; Hor, T. S. A. In *Ferrocenes—Homogeneous Catalysis, Organic Synthesis, Materials Science*; Togni, A., Hayashi, T., Eds.; VCH: Weinheim, FRG, 1995; pp 3–104.

(6) Chaudret, B.; Delavaux, B.; Poilblanc, R. *Coord. Chem. Rev.* **1988**, *86*, 191–243.

(7) Simpson, R. D.; Bergman, R. G. *Organometallics* **1992**, *11*, 3980–3993. Simpson, R. D.; Bergman, R. G. *Organometallics* **1992**, *11*, 4306–4315. Simpson, R. D.; Bergman, R. G. *Angew. Chem., Int. Ed. Engl.* **1992**, *31*, 220–223. Simpson, R. D.; Bergman, R. G. *Organometallics* **1993**, *12*, 781–796. Mandal, S. K.; Ho, D. M.; Orchin, M. *Organometallics* **1993**, *12*, 1714–1719; Mandal, S. K.; Ho, D. M.; Orchin, M. *Polyhedron* **1992**, *11*, 2055–2063.

be maintained, the conformational differences of the bridging diphosphines in relation to the methoxy bridges would then be a subject of great interest. Apart from our recent report of the solution dynamics of **1**,<sup>8</sup> we are not aware of such a study in the literature. Such dynamic studies could not be satisfactorily done without structural data. In this context, we also report the X-ray crystal structure of  $\text{Re}_2(\mu\text{-OMe})_2(\mu\text{-dppm})(\text{CO})_6$  and its NMR behavior in solution. Although dppm and dppf appear to share little similarities apart from being difunctional phosphines, some of their dinuclear and polynuclear complexes have common structural characteristics.<sup>9</sup> Comparisons of the structural data of **1** and **2** would give us the first insight into the different effects of these two phosphines in identical bridging environments. On the basis of these structural data, we can also carry out a molecular modeling study on the fluxional behavior of these complexes in solution. In the course of our study, some unusual features were observed in the <sup>1</sup>H NMR spectrum of **3**. We traced this to an unexpected aggregation, which is revealed by dynamic laser-light scattering (DLS). Similar applications of DLS in biomolecules,<sup>10</sup> polymers,<sup>11</sup> surface films,<sup>12</sup> optics,<sup>13</sup> chromatography,<sup>14</sup> and other fluids and particles<sup>15</sup> have attracted vigorous attention recently but such study in organometallics is limited.

## Results and Discussion

Oxidative decarbonylation of  $\text{Re}_2(\text{CO})_{10}$  at room temperature by  $\text{Me}_3\text{NO}$  in a THF/MeOH mixture gives an "activated" mixture, which upon addition of free diphosphine (PP = dppm (**2**), dppe (**3**), dppp (**4**), dppb (**5**)) results in  $\text{Re}_2(\mu\text{-OMe})_2(\mu\text{-PP})(\text{CO})_6$  in **34**, **29**, **28**, and **10%** yields respectively.<sup>16</sup> The IR spectra, which are in excellent agreement with the spectrum of the dppf analogue, are suggestive of *fac*-Re(I) tricarbonyl moi-

eties. Proton NMR resonances due to the bridging methoxy protons lie in a narrow range 4.29–4.34 ppm, which is in close agreement with those of the dppf analogue (4.59 ppm). These data, supported further by the characteristic low-field <sup>13</sup>C NMR shifts of the bridging methoxy carbon (72.55–73.27 ppm), suggest that the title complexes are isostructural with the dppf analogue. Molecular weight data are in general agreement with a dinuclear structure. These give the first indication that the synthetic route is applicable to all the diphosphines used and that the dinuclear structure is maintained regardless of the phosphine chain lengths.

A related terminal methoxy complex,  $\text{Re}(\text{OMe})(\eta^2\text{-dppe})(\text{CO})_3$ , prepared from the metathesis of *fac*- $\text{Re}(\text{OTs})(\text{CO})_3(\text{dppe})$  with NaOMe, has been recently reported.<sup>17</sup> There is no evidence that a similar mononuclear complex with a chelating diphosphine is formed under our synthetic conditions. This can be ascribed to different formation mechanisms for both syntheses. There is evidence that the bis(methoxy)-bridged precursor  $\text{Re}_2(\mu\text{-OMe})_2(\text{CO})_8$  is formed in the activated mixture.<sup>18</sup> The <sup>1</sup>H NMR spectrum of this mixture shows an intense resonance at 4.87 ppm, which may be attributed to a methoxy bridge.<sup>19</sup> This key intermediate undergoes phosphine substitution to give the observed products. Once these dirhenium complexes are formed, they are stabilized by three bridging ligands and hence show little tendency to dissociation. Addition of free diphosphine has no effect on the complexes at room temperature, *i.e.*, they do not provide a synthetic passage to  $\text{Re}(\text{OMe})(\eta^2\text{-PP})(\text{CO})_3$ .

For unknown reasons, the spectroscopic (IR and <sup>1</sup>H NMR) data for **2** prepared by our method are slightly different from those for the same complex<sup>4</sup> from the photolysis of  $\text{Re}_2(\mu\text{-dppm})(\text{CO})_8$ .<sup>20</sup> Formation of the literature complex occurs via  $\text{Re}_2(\mu\text{-H})(\mu\text{-OMe})(\text{CO})_6(\mu\text{-dppm})$ . There is no evidence that this hydride is involved in the present synthesis. Notably, **3** (or its precursor,  $\text{Re}_2(\mu\text{-H})(\mu\text{-OMe})(\text{CO})_6(\mu\text{-dppe})$ ) cannot be obtained from  $\text{Re}_2(\text{CO})_8(\mu\text{-dppe})$  under photolytic conditions. Other diphosphine analogues have not been reported. The method used here is hence a more general route to prepare these bridging diphosphine complexes.

The differences in the spectroscopic data for **2** obtained by us and those reported are slight but disturbing. They prompted us to investigate its solid-state structure by X-ray crystallography. It confirms a dimeric framework with dppm and two methoxy ligands bridging two *facial* Re(I) tricarbonyl moieties (Figure 1). The methoxy methyls are pointing away from the dppm group. Replacement of dppf (in **1**) by dppm (in **2**) induces some changes in the bonding characteristics

(8) Lam, S.-L.; Cui, Y.-X.; Au-Yeung, S. C. F.; Yan, Y.-K.; Hor, T. S. A. *Inorg. Chem.* **1994**, *33*, 2407–2412.

(9) Neo, S. P.; Zhou, Z.-Y.; Mak, T. C. W.; Hor, T. S. A. *Inorg. Chem.* **1995**, *34*, 520–523. Neo, S.-P.; Hor, T. S. A.; Zhou, Z.-Y.; Mak, T. C. W. *J. Organomet. Chem.* **1994**, *464*, 113–119.

(10) Wu, C. *Macromolecules* **1993**, *26*, 3821–3825. Wu, C. *J. Polym. Sci. B, Polym. Phys.* **1994**, *32*, 803–810. Kadima, W.; Ogedal, L.; Bauer, R.; Kaarsholm, N.; Brodersen, K.; Hansen, J. F.; Porting, P. *Biopolymers* **1993**, *33*, 1643–1657. Komatsu, H.; Yoshii, K.; Ishimitsu, S.; Okada, S.; Takahata, T. *J. Chromatogr.* **1993**, *644*, 17–24. Burne, P. M.; Sellen, D. B. *Biopolymers* **1994**, *34*, 371–382. Watanabe, Y.; Takagi, T. *J. Chromatogr. A* **1993**, *653*, 241–246.

(11) Wu, C.; Lilge, D. *J. Appl. Polym. Sci.* **1993**, *50*, 1753–1759. Degroot, A. W.; Hamre, W. J. *J. Chromatogr.* **1993**, *648*, 33–39. Sedlacek, J.; Vohlidal, J.; Grubisicgallot, Z. *Makromol. Chem., Rapid Commun.* **1993**, *14*, 51–53. Hsu, C. H.; Peacock, P. M.; Flippen, R. B.; Yue, J.; Epstein, A. J. *Synth. Met.* **1993**, *60*, 223–225. Kasparkova, V.; Ommundsen, E. *Polymer* **1993**, *34*, 1765–1767. Grubisicgallot, Z.; Gallot, Y.; Sedlacek, J. *Macromol. Chem. Phys.* **1994**, *195*, 781–791.

(12) Xu, R. L. *Langmuir* **1993**, *9*, 2955–2962. Yang, K.; Mirabelli, E.; Wu, Z. C.; Schowalter, L. J. *J. Vac. Sci. Tech. B* **1993**, *11*, 1011–1013. Smith, G. W.; Pidduck, A. J.; Whitehouse, C. R.; Gasper, J. L.; Spowart, J. *J. Cryst. Growth* **1993**, *127*, 966–971.

(13) Celii, F. G.; Beam, E. A.; Filessesler, L. A.; Liu, H. Y.; Kao, Y. C. *Appl. Phys. Lett.* **1993**, *62*, 2705–2707. Naqwi, A. A.; Durst, F. *Appl. Optics* **1993**, *32*, 4003–4018.

(14) Mhatre, R.; Krull, I. S. *Anal. Chem.* **1993**, *65*, 283–286. Aitzetmuller, K.; Gronheim, M. *Fett Wiss. Technol.* **1993**, *95*, 164–168. Dayal, U.; Mehta, S. K. *J. Liq. Chromatogr.* **1994**, *17*, 303–316. Mhatre, R.; Qian, R.; Krull, I. S.; Gadam, S.; Cramer, S. M. *Chromatographia* **1994**, *38*, 349–354. Meyer, E. M.; Vasconcellos, S. R. *ACS Symp. Ser.* **1994**, No. 548, 131–143.

(15) Dishman, K. L.; Doolin, P. K.; Hoffman, J. F. *Ind. Eng. Chem. Res.* **1993**, *32*, 1457–1463. Ochi, K.; Momose, M.; Kojima, K.; Lu, B. C. Y. *Can. J. Chem. Eng.* **1993**, *71*, 982–985. Krieger, H.; Schulz, R.; Staude, W. *Exp. Fluids* **1993**, *15*, 240–246.

(16) These yields are generally modest, but the complexes isolated are the principal products and the only ones isolable from the reaction mixtures. Negligible  $\text{Re}_2(\text{CO})_{10}$  is apparent at the end of the reaction.

(17) Mandal, S. K.; Ho, D. M.; Orchin, M. *Inorg. Chem.* **1991**, *30*, 2244–2248.

(18) Yan, Y. K. M.S. Thesis, National University of Singapore, 1992. Hor, T. S. A.; Lam, C. F.; Yan, Y. K. *Bull. Sing. Nat. Int. Chem.* **1991**, *19*, 115–122.

(19) Although  $\text{Re}_2(\text{CO})_8\text{X}_2$  (X = halides) is well-established, there has been no report of such a complex for X = OMe. We are still trying to isolate this proposed intermediate both from the reaction mixture and by another independent synthetic route. Further results will be reported in due course.

(20) Brown et al. reported a weak infrared band at 1893  $\text{cm}^{-1}$  (2027s, 2010 m, 1924 m, 1893 w, 1885 sh). This band is the strongest band in our spectrum. From the reported NMR data, the methylene protons of dppm (3.71 ppm) are more deshielded compared to those of our complex (3.14 ppm). These differences are, however, sufficiently minor that both data sets could infer the structure proposed. Presumably the differences, if any, are conformational in nature.

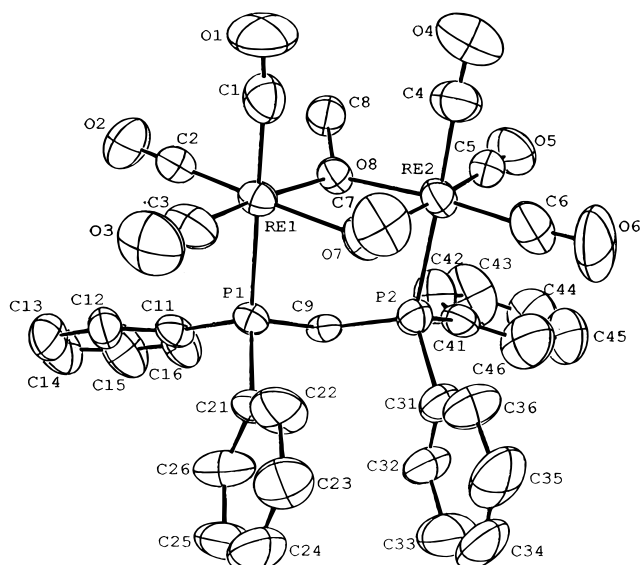


**Figure 1.** ORTEP plot of the molecular structure of  $\text{Re}_2(\mu\text{-OMe})_2[\mu\text{-Ph}_2\text{PCH}_2\text{PPh}_2](\text{CO})_6$  (**2**) (50% probability ellipsoids).

of the central  $\{\text{Re}_2\text{O}_2\}$  core. The Re–O bonds slightly strengthen from 2.163(6) Å in **1** to 2.143(8) Å in **2** (mean). While the Re–O–Re angles remain fairly constant ( $103.9(2)^\circ$  in **1** and  $104.7(3)^\circ$  in **2** (mean)), the O–Re–O angles open up (from  $71.3(2)^\circ$  in **1** to  $74.8(3)^\circ$  in **2** (mean)), presumably as a result of the shorter Re–O bonds. However, in supporting this  $\{\text{Re}_2\text{O}_2\}$  core, which is found to be rigid in **1**, the overhead bridge–dppf or dppm–adjusts and adapts according to its own geometric demands. In **1**, the bulk of the dppf bridge forces the centroids of the Cp···Cp axis to twist significantly with respect to the Re···Re axis and the two Re(I) coordination planes to fold along the O···O axis away from the phosphine. These deformations are no longer necessary in **2**, as dppm is more suited as an overhead bridge. Four effects are immediately obvious. (i) The Re–P bonds strengthen significantly from 2.531(2) Å in **1** to 2.482(4) Å in **2**. (ii) In **1**, the P···P vector is roughly parallel to the Re···Re vector (dihedral angles  $\text{Re}(2)\cdots\text{Re}(1)\text{-P}(1)\cdots\text{P}(2) = \text{Re}(1)\cdots\text{Re}(2)\text{-P}(2)\cdots\text{P}(1) = 2.3(1)^\circ$ ); in **2**, it is even more parallel ( $0.6(1)^\circ$ ). The slight tilting of the P···P axis allows more room for the ferrocenyl moiety to fit into the  $[\text{Re}_2(\mu\text{-OMe})_2]$  pocket. (iii) The folding of the  $\{\text{Re}_2\text{O}_2\}$  core is significantly less pronounced in **2** ( $\angle\text{Re-O}\cdots\text{O-Re} = 29.0(2)^\circ$  in **1** and  $9.4(3)^\circ$  in **2**;  $\angle\text{O-Re}\cdots\text{Re-O} = 38.5(3)^\circ$  in **1** and  $12.3(5)^\circ$  in **2**) (see Figure 2A). This freedom to fold provides a leverage for the core to adapt to diphosphines of different steric demands. The Re···Re separation shortens from 3.4042(6) Å in **1** to 3.3917(7) Å in **2** as the  $\{\text{Re}_2\text{O}_2\}$  core becomes more planar. (iv) As a result of the opening up of the hinge angle of the Re–O···O–Re butterfly, the carbonyls *trans* to the phosphines no longer have to bend away to avoid nonbonding contacts ( $\text{P-Re-C} = 167.1(3)^\circ$  and  $\text{Re-C-O} = 170.3(10)^\circ$  in **1**; in **2** they are  $178.3(4)$  and  $176.6(14)^\circ$ , respectively).

Equipped with the above structural data, we can compare the solution dynamics of the title complexes. Molecular models were constructed for **2–4** as shown in Figure 2. Variable temperature  $^1\text{H}$  NMR experiments were carried out for  $\text{Re}_2(\mu\text{-OMe})(\mu\text{-PP})(\text{CO})_6$  (PP = dppm (**2**); dppe (**3**), dppp (**4**)) from 183 to 293 K (Figure 3). The assignment of the  $^1\text{H}$  NMR spectra is given in the structures shown in Figure 2. The results

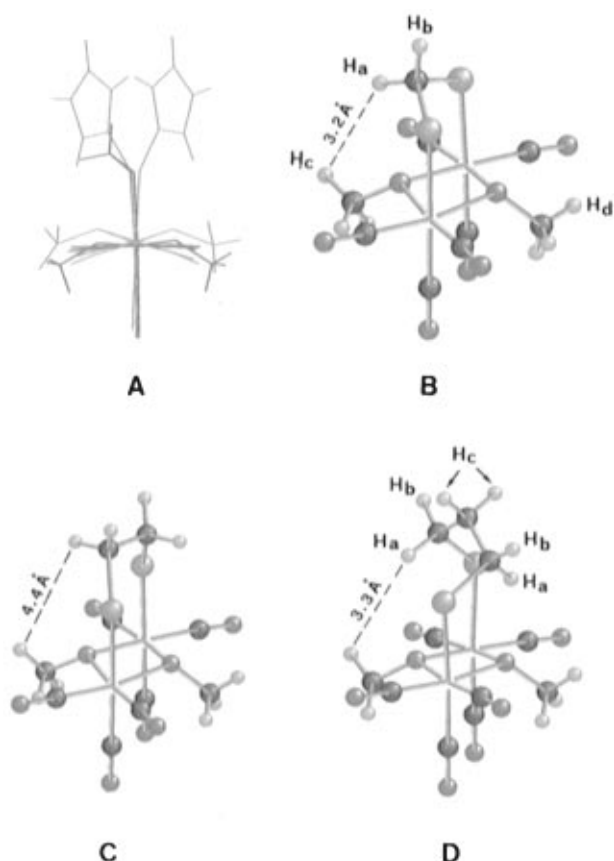


**Figure 2.** (A) Superimposed image of the crystal structures of  $\text{Re}_2(\mu\text{-OMe})_2(\mu\text{-PP})(\text{CO})_6$  (PP = dppf (**1**), and dppm (**2**)). All phenyl rings are hidden. (B–D) Molecular-modeled structures of the dppm, dppe, and dppp complexes, respectively. The dppm complex is based on the single-crystal X-ray structural data of this work. The structures of the dppe and dppp complexes are proposed on the assumption that the bridge fluxionality ceases.

confirmed that the diphosphine bridges of these complexes undergo fluxional motion at room temperature. The frozen configuration of **2** at 183 K, in which the methylene bridge flips to one side of the  $\text{Re}_2\text{P}_2$  plane, possibly corresponds to the solid-state configuration. For **3**, the ethylene bridge undergoes rapid fluxional motion even at 183 K; the four ethylene protons are equivalent in the temperature range studied. This implies the symmetrical disposition of the ethylene bridge with respect to the  $\text{Re}_2\text{P}_2$  plane. In **4**, the appearance of the two inequivalent proton sets ( $\text{H}_a$  and  $\text{H}_b$ ) at 183 K directly confirms the fluxionality of the propylene bridge. This complex is still nonrigid at 183 K. The frozen structure is projected as shown in Figure 2D. In our earlier study of the dppf complex,<sup>8</sup> the fluxionality of the dppf bridge was found to be controlled primarily by the combined effects of torsional strains and the interaction between the ferrocenyl  $\text{C}_5$  planes and phenyl rings. For the present three complexes, the fluxionalities for the conversion of the enantiomers are suggested to be controlled by correlated bond rotation and torsional motion.

Additional features are noted in the  $^1\text{H}$  NMR spectra of **2** and **3**. The methoxo peak in **2** is partially resolved into two inequivalent groups at 183 K. With the methylene bridge tilted to one side of the  $\text{Re}_2\text{P}_2$  plane, the two methoxo groups are differentiable (see Figure 2B) and two resonances begin to emerge at low temperature. Interaction between a methylene proton ( $\text{H}_a$ )

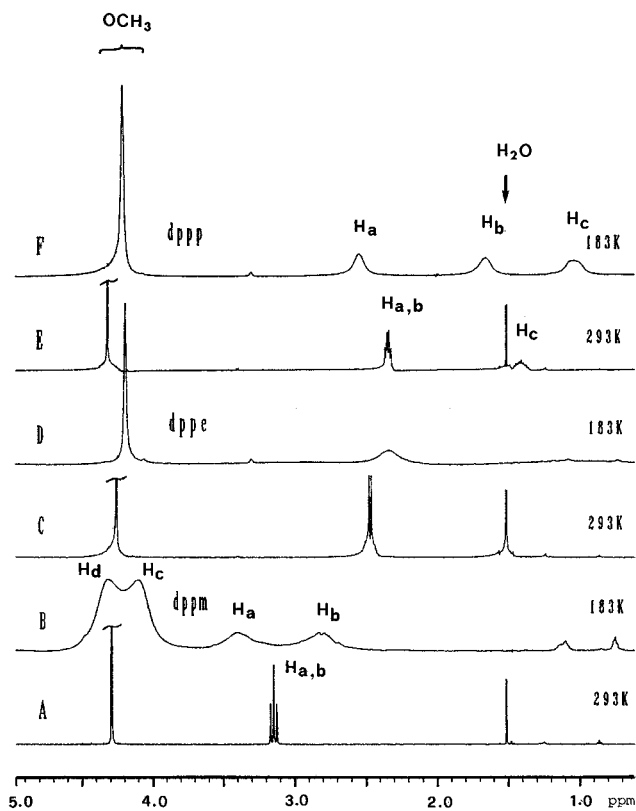


**Figure 3.**  $^1\text{H}$  NMR spectra of  $\text{Re}_2(\mu\text{-OMe})_2(\mu\text{-PP})(\text{CO})_6$  (PP = dppm (A, B), dppe (C, D) and dppp (E, F) at 293 and 183 K. At 293 K,  $\text{H}_a$  and  $\text{H}_b$  are equivalent and the  $^2J_{\text{P-H}_{a,b}}$  values for the dppm and dppe complexes are determined to be 11.4 and 7.8 Hz, respectively. For the dppp complex,  $^3J_{\text{H-H}}$  and  $^2J_{\text{P-H}}$  are determined to be 7.4 and 6.1 Hz, respectively, at 293 K.

in the alkyl bridge and a methoxy proton (shown by the broken lines connecting the proton pairs in Figure 2B) consequently distinguishes it from the other methylene proton ( $\text{H}_b$ ). A similar methylene-methoxy interaction is also expected in **3** (Figure 2C) and **4** (Figure 2D). However, this interaction is stronger in **2** and **4** compared to **3**, as the closest contacts are determined to be 3.2 Å (**2**), 4.4 Å (**3**), and 3.3 Å (**4**). The methoxy protons are not resolved in the  $^1\text{H}$  spectrum of **4**. This can be understood on the basis of the frozen structure (Figure 2D), in which a  $\text{C}_2$  axis is located along the central methylene carbon and the center of the  $\text{Re}_2\text{O}_2$  core. The two methoxy groups are hence equivalent in this model. Relatively normal phosphorus angles,  $\angle\text{C}_{\text{alkyl bridge}}\text{-P-Re}$ , are obtained for **2** ( $\sim 113^\circ$ ) and **4** ( $\sim 118^\circ$ ). For **3**, a surprisingly high value for this angle ( $\sim 144^\circ$ ) suggests large angular strain. It can be relieved if the staggered conformation of the ethylene bridge is relaxed and/or the folding of the  $\{\text{Re}_2\text{O}_2\}$  core is increased.

A second feature to be noted is the  $^1\text{H}$  NMR spectrum of the methylene protons ( $\delta(^1\text{H})$  2.4 ppm) in the dppe complex **3**. It consists of a sharp doublet superimposed on a broad peak with a half-height line width of 0.1 ppm. There was no visible precipitation in the sample when the NMR experiment was completed (minutes). On the basis of the results of both  $^1\text{H}\{^{31}\text{P}\}$  and 2D  $^1\text{H}\text{-}^{31}\text{P}$  COSY experiments, the presence of impurities or byproducts was ruled out. Molecular weight measurement of a fresh solution (toluene) was also consistent with the formulation of a dimeric complex. There is no chemical evidence which could support the breakdown of the  $\{\text{Re}_2\text{O}_2\}$  core to its monomeric form or polymerization

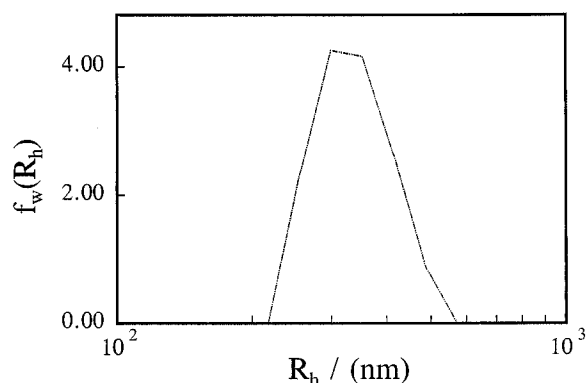


**Figure 4.** Plots of the weight distribution  $f_w(R_h)$  versus the hydrodynamic radius  $R_h$  for the dppe complex after it stood for 2.5 h in solution.

of the complex. One possibility which could account for the anomalous NMR spectral feature is the formation of clusters through association and/or aggregation. To obtain an insight into this observed behavior, dynamic DLS measurements (Appendix) of complexes **2–4** in  $\text{CH}_2\text{Cl}_2$  were carried out. In agreement with the NMR data, there is no aggregate formation for **2** (dppm) but there is a small tendency for **4** (dppp) to aggregate in  $\text{CH}_2\text{Cl}_2$ . For **3** (dppe), the result conclusively confirms the cluster formation on aggregation in dichloromethane. By the end of the first 1 h of data collection, a broad distribution of particles centered at  $R_h \sim 1$  nm is detected. By the end of the 2.5 h period, aggregates are formed with a particle size distribution centered at  $\sim 370$  nm. Since DLS is not very accurate in the size range of 0.2–1  $\mu\text{m}$ , especially when the sample is broadly distributed, our DLS results showed only that there exist some large aggregates in the solution. Figure 4 shows a differential weight distribution of the dppe aggregates after 2.5 h. These results suggest that aggregate formation which gives rise to differences in the local environment is responsible for the broadening in the  $^1\text{H}$  NMR spectrum. The chemical origin of this aggregation is unclear at present, but to our knowledge this is the first experimental evidence for aggregation of an organometallic complex in solution demonstrated by a combination of DLS and NMR.<sup>21</sup> Further work is in progress to elucidate the species responsible for this observed behavior.

The use of amine oxide in stoichiometric decarbonylation is well-known.<sup>22</sup> It has also been reported recently that  $\text{Me}_3\text{NO}$  can induce disproportionation of  $\text{Re}_2(\text{CO})_{10}$ .<sup>23</sup> The present synthesis, however, does not require the stoichiometric presence of amine oxide. The experimentally optimized  $\text{Re}_2:\text{Me}_3\text{NO}$  ratio of 1.0:2.4 is significantly short of the theoretical ratio of 1:4. This

(21) One reviewer kindly drew our attention to the following paper: Nelson, W. H.; Howard, W. F., Jr.; Pecora, R. *Inorg. Chem.* **1982**, *21*, 1483. This work describes the use of depolarized Rayleigh scattering in the study of Rayleigh intensity line shapes for  $\text{SnBu}_2(\text{dbzm})_2$  and  $\text{Sn}(\text{Cyhex})(\text{dbzm})_2$  (dbzm = dibenzoylmethane). It gives information on the structure and geometry of the complexes but bears little relation to our work.

(22) Albers, M. O.; Coville, N. J. *Coord. Chem. Rev.* **1984**, *53*, 227–259. Luh, T.-Y. *Coord. Chem. Rev.* **1984**, *60*, 255–276. Hor, T. S. A.; Chan, H. S. O.; Tan, K. L.; Phang, L.-T.; Yan, Y. K.; Liu, L.-K.; Wen, Y.-S. *Polyhedron* **1991**, *10*, 2437–2450. Hor, T. S. A.; Phang, L.-T. *J. Organomet. Chem.* **1989**, *373*, 319–324. Hor, T. S. A. *J. Organomet. Chem.* **1988**, *340*, 51–57. Hor, T. S. A.; bte Rus, S. R. *J. Organomet. Chem.* **1988**, *348*, 343–347. Shen, J.-K.; Gao, Y.-C.; Shi, Q.-Z.; Basolo, F. *Coord. Chem. Rev.* **1993**, *128*, 69–88 and references therein.

(23) Christie, S. D.; Clerk, M. D.; Zaworotko, M. J. *J. Crystallogr. Spectrosc. Res.* **1993**, *23*, 591–594.

is not surprising, as nucleophilic substitution of carbonyl can be induced by methoxo attack. Carbonyl labilization can also be promoted by methoxycarbonyl<sup>24</sup> formation (from direct attack of methoxide on the carbonyl carbon<sup>25</sup>). When more Me<sub>3</sub>NO is added, or when the mixture is doped with NEt<sub>3</sub> in a hope to promote further decarbonylation, the product yields are significantly lower. We attribute this to the formation under these conditions of the tribridged species [Re<sub>2</sub>(μ-OMe)<sub>3</sub>(CO)<sub>6</sub>]<sup>-</sup>,<sup>26</sup> which does not easily undergo substitution with the diphosphine to give the desired product.

The low yield of the dppb complex **5** is indicative of the upper limit of the chain length of the diphosphine which can be tolerated by the Re<sub>2</sub>(μ-OMe)<sub>2</sub> core. In agreement with this, the use of diphosphines with longer chain length, namely, bis(diphenylphosphino)pentane and -hexane, failed to give any major characterizable products. What seems surprising is that the use of PPh<sub>3</sub> in these syntheses gives no isolable products except Re<sub>2</sub>(CO)<sub>10-n</sub>(PPh<sub>n</sub>) (*n* = 1–3) in low yields. There is no evidence for the formation of the expected product Re<sub>2</sub>(μ-OMe)<sub>2</sub>(PPh<sub>3</sub>)<sub>2</sub>(CO)<sub>6</sub>. The importance of the bridging diphosphine in the stabilization of these methoxo-bridged complexes is thus evident.

### Conclusions

The Re<sub>2</sub>(μ-OMe)<sub>2</sub>(μ-PP)(CO)<sub>6</sub> system proved to be a good model for structural and solution dynamic comparisons for bridging diphosphines in a dinuclear frame. The facile assembly and geometrical tolerance of the Re<sub>2</sub>(μ-OMe)<sub>2</sub> core are unexpected. This has encouraged us to examine other related alkoxo systems; these studies are presently in progress. What seems most surprising is the aggregation phenomenon and its verification by DLS. The potential of DLS in organometallics is rich and awaits further exploitation. What we reported here may not be a rare phenomenon, and perhaps there should be reexamination of some of the abnormal NMR peak broadenings in many literature complexes in light of the present findings.

### Experimental Section

**General Considerations.** All reactions were performed under Ar using standard Schlenk techniques. Chemical reagents were supplied from commercial sources and used without further purification. Trimethylamine oxide (TMNO) are used in its dihydrate form. Precoated silica plates of layer thickness 0.25 mm were obtained from Merck or Baker. Solvents used were reagent grade and were freshly distilled under N<sub>2</sub> before use. <sup>1</sup>H NMR spectra were recorded on a Bruker ARX-500 superconducting FT-NMR spectrometer operating at a proton frequency of 500.13 MHz. All complexes were dissolved in 0.5 mL of 99.6% CD<sub>2</sub>Cl<sub>2</sub>. The chemical shift was referenced to the residual CH<sub>2</sub>Cl<sub>2</sub> signal, which was set at 5.3 ppm at room temperature. Variable-temperature NMR measurements were made after the sample was equilibrated for 1 h at 293, 253, 223, 203, 193, 188, and 183 K. <sup>31</sup>P NMR spectra were recorded on a Bruker ACF 300 MHz spectrometer at 121.50 MHz. Chemical shifts are reported in ppm to a high frequency of external H<sub>3</sub>PO<sub>4</sub>. <sup>13</sup>C NMR spectra were recorded

on a Bruker AMX-500 spectrometer at 125.76 MHz. All IR spectra were recorded in CHCl<sub>3</sub> solution on an FT-IR Perkin-Elmer 1600 spectrometer. Elemental analyses were performed by the microanalytical laboratory of the Chemistry Department at the National University of Singapore. Molecular weight determination was carried out by vapor-pressure osmometry in a Knauer–Dampfdruck osmometer by Galbraith Laboratories, Inc., in Knoxville, TN, using toluene as solvent. The presence of CH<sub>2</sub>Cl<sub>2</sub> as a solvate molecule was confirmed by NMR spectroscopy of the sample solutions in CDCl<sub>3</sub>.

**Molecular Modeling Studies.** All molecular modeling work was carried out on a Silicon Graphics Indigo II Extreme workstation using the software SYBYL (version 6.04) licensed from Tripos Associates Inc., St. Louis, MO. Single-crystal X-ray data were used for the construction of the dppm and dppf complexes in Figure 2. For the construction of the dppe and dppp analogues, standard bond lengths and angles were used. Typical bond lengths and the associated angles were used for the C–H and C–P bonds. The Re–P distance of the dppm complex was used to construct the dppe and dppp counterparts. Furthermore, it was assumed that (i) the Re<sub>2</sub>O<sub>2</sub> core of the dppe and dppp complexes is similar to that of the dppm complex and (ii) the ethylene and propylene bridges adopt the staggered (thermodynamically more stable) conformation. Support for the validity of these assumptions is derived from the variable-temperature <sup>1</sup>H NMR spectra for both dppe and dppp complexes. A least-squares method was used to fit the Re<sub>2</sub>O<sub>2</sub> core of the dppm complex with that of the dppf analogue.

**Dynamic Laser-Light Scattering (DLS) Instrumentation and Measurements.** For dynamic DLS measurements of the dppe complex, the sample was prepared in CH<sub>2</sub>Cl<sub>2</sub> at the same concentration (5 mg/mL) at which the NMR spectrum was recorded. It was then filtered through a Millipore 0.5 μm LCR filter for dust removal. A commercial DLS spectrometer (ALV-5000, Langen in Hessen, Germany) equipped with a fast correlator card (minimum sample time is 12.5 ns) was used for measurements. A Nd:YAG laser (ADLAS DPY 42511) operated at 532 nm and 400 mW was used as the light source. The primary beam was vertically polarized. Scattered intensity was taken at 45° to the incident beam. With this DLS spectrometer, we are able to determine the particle size down to 1 nm. Details of the instrumentation employed in this study have been published elsewhere.<sup>27</sup> The correlation function was accumulated until the difference between the measured and calculated base lines was less than 0.1%. In this study, the measured average line width ⟨Γ⟩ was linearly scaled by the square of the scattering vector *q*, namely ⟨Γ⟩ ∝ *q*<sup>2</sup>, which indicated that the relaxation is diffusive. To extract the diffusion coefficient *D* (see Appendix), *G*(Γ) is calculated by using the Laplace inversion program CONTIN.<sup>28</sup> For readers who are unfamiliar with the DLS technique, we have included in the Appendix some detailed information. For the calculation of the hydrodynamic radius *R*<sub>h</sub> in CH<sub>2</sub>Cl<sub>2</sub>, a value of 0.433 was used for the viscosity η.

**Synthesis. Re<sub>2</sub>(μ-OMe)<sub>2</sub>(μ-dppm)(CO)<sub>6</sub> (2).** Separation by TLC (CH<sub>2</sub>Cl<sub>2</sub>/hexane, 1:4) after reaction of TMNO·2H<sub>2</sub>O (0.164 g, 1.47 mmol), Re<sub>2</sub>(CO)<sub>10</sub> (0.400 g, 0.61 mmol) and dppm (0.236 g, 0.61 mmol) gave fine white crystals of Re<sub>2</sub>(μ-OMe)<sub>2</sub>(μ-dppm)(CO)<sub>6</sub> (mp 207–208 °C) as the main product after recrystallization with CH<sub>2</sub>Cl<sub>2</sub>/hexane (0.205 g, 34%). IR: ν(CO) 2027 vs, 2013 s, 1927 m, 1912 m, 1895 vs cm<sup>-1</sup> (toluene). <sup>1</sup>H NMR: δ 7.36–7.19 (m, 20H, Ph), 4.32 (s, 6H, OMe), 3.14 (t, 2H, CH<sub>2</sub>, <sup>2</sup>J<sub>F-H</sub> = 11.3 Hz). <sup>31</sup>P NMR δ 9.67 (s). <sup>13</sup>C NMR: δ 14.30 (t, CH<sub>2</sub>, J<sub>C-P</sub> = 9.2 Hz), 74.83 (s, OMe), 128.71 (d, Ph, C<sub>meta</sub>, J<sub>C-P</sub> = 9.5 Hz), 130.67 (s, Ph, C<sub>para</sub>), 132.40 (d, Ph, CH, J<sub>C-P</sub> = 48.0 Hz), 132.40 (d, Ph, C<sub>ortho</sub>, J<sub>C-P</sub> = 11.4), 194.22 (d, CO *trans* P, J<sub>C-P</sub> = 83.3 Hz), 196.09 (s, CO *cis* P). Anal. Calcd for C<sub>33</sub>H<sub>28</sub>O<sub>8</sub>P<sub>2</sub>Re<sub>2</sub>: C, 40.16; H, 2.86; P, 6.28. Found: C, 40.13; H, 2.63; P, 6.38.

**Re<sub>2</sub>(μ-OMe)<sub>2</sub>(μ-dppe)(CO)<sub>6</sub>·CH<sub>2</sub>Cl<sub>2</sub> (3).** A solution of

(24) Darensbourg, D. J. *Adv. Organomet. Chem.* **1982**, *21*, 113–150.

(25) Angelici, R. J. *Acc. Chem. Res.* **1972**, *5*, 335–341. Gross, D. C.; Ford, P. C. *J. Am. Chem. Soc.* **1985**, *107*, 585–593. Trautman, R. J.; Gross, D. C.; Ford, P. C. *J. Am. Chem. Soc.* **1985**, *107*, 2355–2362.

(26) Freni, M.; Romiti, P. *Atti Accad. Naz. Lincei, Mem., Cl. Sci. Fis., Mat. Nat., Rend.* **1973**, *55*, 515. Ginsberg, A. P.; Hawkes, M. J. *J. Am. Chem. Soc.* **1968**, *90*, 5930–5932.

(27) Wu, C.; Xia, K. Q. *Rev. Sci. Instrum.* **1994**, *65*, 587–590.

(28) Provencher, S. W. *Biophys. J.* **1976**, *16*, 29; *J. Chem. Phys.* **1976**, *64*, 2772–2777; *Makromol. Chem.* **1979**, *180*, 201.

TMNO·2H<sub>2</sub>O (0.060 g, 0.54 mmol) in THF/MeOH (1:1; 20 cm<sup>3</sup>) was transferred to a stirred solution of Re<sub>2</sub>(CO)<sub>10</sub> (0.150 g, 0.23 mmol) in 20 cm<sup>3</sup> of THF. The resultant yellow solution was stirred *in vacuo* for 4 h at room temperature. Solid dppe (0.092 g, 0.23 mmol) was added. The reaction mixture was stirred for 1 h *in vacuo*, after which half the volume of solvent was removed and the solution was further stirred for 3 h under Ar. The solution was evaporated to dryness and the residue redissolved in the minimum amount CH<sub>2</sub>Cl<sub>2</sub>. Separation by TLC using CH<sub>2</sub>Cl<sub>2</sub>/hexane (1:4) as eluent affords fine white crystals of Re<sub>2</sub>(μ-OMe)<sub>2</sub>(CO)<sub>6</sub>(μ-dppe)·CH<sub>2</sub>Cl<sub>2</sub> (mp 204–206 °C dec) after recrystallization with CH<sub>2</sub>Cl<sub>2</sub>/hexane (0.067 g, 29%). IR: ν(CO) 2026 vs, 2010 s, 1925 m, 1903 vs (sh), 1890 vs (br) cm<sup>-1</sup>. <sup>1</sup>H NMR (CDCl<sub>3</sub>) δ 7.47–7.50 (m, 20H, Ph), 5.30 (s, 2H, CH<sub>2</sub>Cl<sub>2</sub>), 4.29 (s, 6H, OMe), 2.47 (d, 4H, CH<sub>2</sub>, <sup>2</sup>J<sub>P-H</sub> = 7.8 Hz). <sup>31</sup>P NMR: δ 15.24 (s). <sup>13</sup>C NMR: δ 16.60 (d, CH<sub>2</sub>CH<sub>2</sub>, J<sub>C-P</sub> = 21.4 Hz), 73.27 (s, OMe), 128.90 (s, Ph, C<sub>meta</sub>), 130.75 (s, Ph, C<sub>para</sub>), 132.48 (s, Ph, C<sub>ortho</sub>), 133.66 (d, Ph, C-P, J<sub>C-P</sub> = 44.1 Hz), 193.82 (d, CO *trans* P, J<sub>C-P</sub> = 83.2 Hz), 195.59 (s, CO *cis* P). Mol wt: found, 1042; calcd, 1003. Anal. Calcd for C<sub>35</sub>H<sub>32</sub>Cl<sub>2</sub>P<sub>2</sub>O<sub>8</sub>Re<sub>2</sub>: C, 38.72; H, 2.97; P, 5.71. Found: C, 38.97; H, 2.90; P, 6.43.

**Re<sub>2</sub>(μ-OMe)<sub>2</sub>(μ-dppp)(CO)<sub>6</sub> (4).** The dppp analogue was prepared in the same manner from TMNO·2H<sub>2</sub>O (0.125 g, 1.13 mmol), Re<sub>2</sub>(CO)<sub>10</sub> (0.301 g, 0.46 mmol) and dppp (0.189 g, 0.46 mmol). Separation by TLC (CH<sub>2</sub>Cl<sub>2</sub>/hexane, 35:65) gave Re<sub>2</sub>(μ-OMe)<sub>2</sub>(μ-dppp)(CO)<sub>6</sub> as the main product after recrystallization from a CH<sub>2</sub>Cl<sub>2</sub>/hexane mixture (0.133 g, 28%). IR: ν(CO) 2026 vs, 2009 s, 1924 m, 1902 vs (sh), 1892 vs (br) cm<sup>-1</sup>. <sup>1</sup>H NMR: δ 7.41–7.50 (m, 20H, Ph), 4.34 (s, 6H, OMe), 2.35 (dt, 4H<sub>ab</sub>, <sup>2</sup>J<sub>P-H</sub> = 6.1 Hz, <sup>3</sup>J<sub>H<sub>a</sub>-H<sub>b</sub></sub> = 7.4 Hz), 1.44 (m, 2H<sub>c</sub>). <sup>31</sup>P NMR δ 11.43 (s). <sup>13</sup>C NMR: δ 18.44 (s, CH<sub>3</sub>), 21.18 (dd, CH<sub>ab</sub>, J<sub>C-P</sub> = 16.4 Hz, J<sub>C-P'</sub> = 4.4 Hz), 72.55 (s, OMe), 128.64 (d, Ph, C<sub>meta</sub>, J<sub>C-P</sub> = 9.2 Hz), 130.37 (s, Ph, C<sub>para</sub>), 132.72 (d, Ph, C<sub>ortho</sub>, J<sub>C-P</sub> = 10.2 Hz), 135.00 (d, Ph, C-P, J<sub>C-P</sub> = 42.9 Hz), 193.96 (d, CO *trans* P, J<sub>C-P</sub> = 81.3 Hz), 195.27 (d, CO *cis* P, J<sub>C-P</sub> = 6.2 Hz). Mol wt: found, 1046; calcd, 1017. Anal. Calcd for C<sub>35</sub>H<sub>32</sub>P<sub>2</sub>O<sub>8</sub>Re<sub>2</sub>: C, 41.41; H, 3.18; P, 6.10. Found: C, 41.38; H, 3.15; P, 6.22.

**Re<sub>2</sub>(μ-OMe)<sub>2</sub>(μ-dppb)(CO)<sub>6</sub>·CH<sub>2</sub>Cl<sub>2</sub> (5).** Separation by TLC (CH<sub>2</sub>Cl<sub>2</sub>/hexane, 1:1) from a mixture of TMNO·2H<sub>2</sub>O (0.125 g, 1.13 mmol), Re<sub>2</sub>(CO)<sub>10</sub> (0.301 g, 0.46 mmol), and dppb (0.197 g, 0.46 mmol) yielded Re<sub>2</sub>(μ-OMe)<sub>2</sub>(μ-dppb)(CO)<sub>6</sub>·1/2CH<sub>2</sub>Cl<sub>2</sub> as the main isolable product (0.020 g, 10%). IR: ν(CO) 2024 vs, 2007 s, 1921 m, 1896 vs (br) cm<sup>-1</sup>. <sup>1</sup>H NMR: δ 7.47–7.38 (m, 20H, Ph), 5.30 (s, 1H, CH<sub>2</sub>Cl<sub>2</sub>), 4.25 (s, 6H, OMe), 2.52 (dt, 4H<sub>outer</sub>, <sup>2</sup>J<sub>P-H</sub> = 7.9 Hz, <sup>3</sup>J<sub>H-H</sub> = 6.9 Hz), 1.50 (m, 4H<sub>inner</sub>). <sup>31</sup>P NMR: δ 8.35 (s). Mol wt: found, 1383; calcd, 1032. Anal. Calcd for C<sub>36.5</sub>H<sub>35</sub>Cl<sub>0.5</sub>P<sub>2</sub>O<sub>8</sub>Re<sub>2</sub>: C, 40.91; H, 3.29; P, 5.78. Found: C, 40.85; H, 3.17; P, 6.12.

**Reaction of Re<sub>2</sub>(CO)<sub>10</sub> with PPh<sub>3</sub>.** Re<sub>2</sub>(CO)<sub>10</sub> (0.271 g, 0.42 mmol) was mixed and reacted with PPh<sub>3</sub> (0.213 g, 0.81 mmol) in a similar manner for *ca.* 18 h. Separation by TLC (CH<sub>2</sub>Cl<sub>2</sub>/hexane, 1:4) yielded four products. In decreasing *R<sub>f</sub>* value, the first major band is unreacted PPh<sub>3</sub>. The second band on recrystallization with CH<sub>2</sub>Cl<sub>2</sub>/hexane gave Re<sub>2</sub>(CO)<sub>9</sub>(PPh<sub>3</sub>) (0.016 g, 4%). IR: ν(CO) 2105 w, 2033 w, 1995 vs, 1960 w, 1936 m cm<sup>-1</sup> (CH<sub>2</sub>Cl<sub>2</sub>). <sup>1</sup>H NMR: δ 7.42–7.47 (m, 15H, Ph). <sup>31</sup>P NMR δ 15.53 (s). Anal. Calcd for C<sub>27</sub>H<sub>15</sub>O<sub>9</sub>PRe<sub>2</sub>: C, 36.57; H, 1.70. Found: C, 36.53; H, 1.73. The third band is Re<sub>2</sub>(CO)<sub>8</sub>(PPh<sub>3</sub>)<sub>2</sub> (0.005 g, 1%). IR: ν(CO) 2006 w, 1955 s cm<sup>-1</sup> (CH<sub>2</sub>Cl<sub>2</sub>). <sup>1</sup>H NMR δ 7.36–7.50 (m, 30H, Ph). <sup>31</sup>P NMR: δ 17.61 (s). Anal. Calcd for C<sub>42</sub>H<sub>30</sub>O<sub>8</sub>P<sub>2</sub>Re<sub>2</sub>: C, 45.98; H, 2.75. Found: C, 46.90; H, 2.59. The final band was Re<sub>2</sub>(CO)<sub>7</sub>(PPh<sub>3</sub>)<sub>3</sub> (0.012 g, 2%). IR: ν(CO) 2107 w, 2017 (sh) m, 2004 m, 1950 vs, 1906 m cm<sup>-1</sup> (CH<sub>2</sub>Cl<sub>2</sub>); <sup>1</sup>H NMR δ 7.16–7.47 (m, 30H, Ph), 7.62–7.70 (m, 15H, Ph). <sup>31</sup>P NMR: δ 9.07 (s), 6.19 (s). Anal. Calcd for C<sub>62.5</sub>H<sub>48.5</sub>O<sub>7</sub>P<sub>3</sub>Re<sub>2</sub>: C, 54.52; H, 3.55. Found: C, 55.78; H, 3.57.

**Crystal Structure Determination of [Re<sub>2</sub>(μ-OMe)<sub>2</sub>(μ-dppm)(CO)<sub>6</sub>] (2).** Single colorless crystals suitable for an X-ray diffraction study were grown from a sample solution in a mixture of CH<sub>2</sub>Cl<sub>2</sub>/hexane at ~-20 °C. Crystal data:

**Table 1. Crystallographic Data for [Re<sub>2</sub>(μ-OMe)<sub>2</sub>(μ-dppm)(CO)<sub>6</sub>] (2)**

chem formula:	[Re <sub>2</sub> (μ-OMe) <sub>2</sub> (μ-Ph <sub>2</sub> PCH <sub>2</sub> PPh <sub>2</sub> )(CO) <sub>6</sub> ]
fw:	986.93
space group:	<i>P</i> 4 <sub>1</sub>
<i>a</i> =	16.686(1) Å
<i>b</i> =	16.686(1) Å
<i>c</i> =	12.547(1) Å
α =	90°
β =	90°
γ =	90°
<i>V</i> =	3493.3(3) Å <sup>3</sup>
<i>Z</i> =	4
<i>T</i> =	25 °C
λ =	0.709 30 Å
ρ <sub>calcd</sub> =	1.877 g cm <sup>-3</sup>
μ =	7.15 mm <sup>-1</sup>
<i>R</i> ( <i>F</i> <sub>o</sub> ) <sup>a</sup> =	0.021
<i>R</i> <sub>w</sub> ( <i>F</i> <sub>o</sub> ) <sup>b</sup> =	0.024

$$^a R = \sum ||F_o| - |F_c|| / \sum |F_o|. \quad ^b R_w = [\sum w(|F_o| - |F_c|)^2 / \sum w|F_o|^2]^{1/2}.$$

**Table 2. Selected Final Fractional Coordinates for [Re<sub>2</sub>(μ-OMe)<sub>2</sub>(CO)<sub>6</sub>(μ-dppm)] (2)**

atom	<i>x</i>	<i>y</i>	<i>z</i>
Re(1)	0.03093(3)	0.74524(3)	0.15514
Re(2)	0.14215(3)	0.61457(3)	0.30004(5)
P(1)	0.14623(17)	0.75811(17)	0.03079(30)
P(2)	0.2480(2)	0.63550(18)	0.16447(35)
O(1)	-0.1116(7)	0.7359(8)	0.3118(12)
O(2)	0.0034(6)	0.9260(6)	0.1612(12)
O(3)	-0.0957(7)	0.7296(8)	-0.0175(10)
O(4)	0.0118(7)	0.5928(8)	0.4712(10)
O(5)	0.2624(7)	0.6396(7)	0.4808(8)
O(6)	0.1682(8)	0.4339(6)	0.3163(13)
O(7)	0.0632(4)	0.6205(4)	0.1644(8)
O(8)	0.1216(4)	0.7390(4)	0.2745(6)
C(1)	-0.0562(8)	0.7365(8)	0.2541(13)
C(2)	0.0161(7)	0.8576(8)	0.1588(11)
C(3)	-0.0472(8)	0.7377(9)	0.0457(13)
C(4)	0.0604(10)	0.6021(9)	0.4048(14)
C(5)	0.2174(8)	0.6275(7)	0.4127(12)
C(6)	0.1586(9)	0.5035(8)	0.3069(13)
C(7)	-0.0011(9)	0.5626(8)	0.1568(15)
C(8)	0.1195(9)	0.7929(8)	0.3647(10)
C(9)	0.2432(6)	0.7330(6)	0.0966(9)

C<sub>33</sub>H<sub>28</sub>O<sub>8</sub>P<sub>2</sub>Re<sub>2</sub>, *M<sub>r</sub>* = 986.93, tetragonal, *a* = 16.686(1) Å, *c* = 12.547(1) Å, *V* = 3493.3(3) Å<sup>3</sup>, *Z* = 4, *D<sub>c</sub>* = 1.877 Mg m<sup>-3</sup>, *F*(000) = 1879.47, μ(Mo K<sub>α</sub>) = 7.15 mm<sup>-1</sup>, λ = 0.709 30 Å. The space group determined from the systematic absences, is *P*4<sub>1</sub>. The crystal dimensions are 0.16 × 0.19 × 0.38 mm. Cell dimensions were obtained from 25 reflections with 2θ in the range 16.20–36.20°.

**Data Collection and Processing.** A Nonius diffractometer in the θ–2θ mode, with graphite-monochromated Mo K<sub>α</sub> radiation, was used. A total of 2599 reflections was measured, of which 2407 were unique. Data were collected at 298 K to a maximum 2θ value of 44.8°. The ranges of indices were *h* 0–17, *k* 0–17, and *l* 0–13. The diffraction intensities were measured with background counts made for half the total scan time on each side of the peak. Three standard reflections, remeasured after every 1 h, showed no significant decrease in intensity during the data collection. After corrections for Lorentz–polarization and absorption effects (empirical  $\psi$  corrections), 2056 data were used with *I* > 3.0σ(*I*). The minimum and maximum transmission factors were 0.920 and 0.998.

**Structural Analysis and Refinement.** The structure was solved by direct methods and MULTAN.<sup>29</sup> Refinement was by full-matrix least-squares calculations with all non-hydrogen atoms allowed anisotropic motion. All hydrogen atoms were fixed as isotropic ellipsoids in the final cycles of least-squares refinement. The last least-squares cycle was calculated with

(29) Main, P.; Fiske, S. E.; Hull, S. L.; Germain, G.; Declercq, J. P.; Woolfson, M. H. In MULTAN, a System of Computer Programs for Crystal Structure Determination from X-ray Diffraction Data; Universities of York and Louvain, 1980.

**Table 3. Selected bond lengths (Å) and Angles (deg) and Torsional Angles (deg) for [Re<sub>2</sub>(μ-Ome)<sub>2</sub>(CO)<sub>6</sub>(μ-dppm)] (2)**

Bond Distances			
Re(1)–P(1)	2.486(3)	Re(2)–C(6)	1.876(14)
Re(1)–O(7)	2.154(7)	P(1)–C(9)	1.864(11)
Re(1)–O(8)	2.132(8)	P(2)–C(9)	1.838(11)
Re(1)–C(1)	1.917(16)	O(1)–C(1)	1.175(19)
Re(1)–C(2)	1.892(13)	O(2)–C(2)	1.160(16)
Re(1)–C(3)	1.897(15)	O(3)–C(3)	1.142(19)
Re(2)–P(2)	2.477(4)	O(4)–C(4)	1.174(21)
Re(2)–O(7)	2.154(9)	O(5)–C(5)	1.156(19)
Re(2)–O(8)	2.129(7)	O(6)–C(6)	1.177(17)
Re(2)–C(4)	1.905(17)	O(7)–C(7)	1.446(14)
Re(2)–C(5)	1.902(16)	O(8)–C(8)	1.445(14)
Re(1)–Re(2)	3.3917(7)		
Bond Angles			
P(1)–Re(1)–O(7)	85.64(22)	O(7)–Re(2)–C(6)	99.8(5)
P(1)–Re(1)–O(8)	84.03(21)	O(8)–Re(2)–C(4)	95.4(5)
P(1)–Re(1)–C(1)	178.4(4)	O(8)–Re(2)–C(5)	96.1(4)
P(1)–Re(1)–C(2)	91.8(4)	O(8)–Re(2)–C(6)	173.9(5)
P(1)–Re(1)–C(3)	94.8(4)	C(4)–Re(2)–C(5)	88.4(7)
O(7)–Re(1)–O(8)	74.8(3)	C(4)–Re(2)–C(6)	88.0(7)
O(7)–Re(1)–C(1)	94.7(5)	C(5)–Re(2)–C(6)	89.0(6)
O(7)–Re(1)–C(2)	171.7(4)	Re(1)–P(1)–C(9)	112.0(4)
O(7)–Re(1)–C(3)	98.4(5)	Re(2)–P(2)–C(9)	114.3(3)
O(8)–Re(1)–C(1)	94.6(5)	Re(1)–O(7)–Re(2)	103.9(3)
O(8)–Re(1)–C(2)	97.1(4)	Re(1)–O(7)–C(7)	117.1(8)
O(8)–Re(1)–C(3)	173.2(5)	Re(2)–O(7)–C(7)	118.4(9)
C(1)–Re(1)–C(2)	87.7(6)	Re(1)–O(8)–Re(2)	105.5(3)
C(1)–Re(1)–C(3)	86.7(6)	Re(1)–O(8)–C(8)	120.2(7)
C(2)–Re(1)–C(3)	89.6(6)	Re(2)–O(8)–C(8)	119.5(7)
P(2)–Re(2)–O(7)	83.53(23)	Re(1)–C(1)–O(1)	175.5(13)
P(2)–Re(2)–O(8)	82.77(21)	Re(1)–C(2)–O(2)	177.1(11)
P(2)–Re(2)–C(4)	178.2(4)	Re(1)–C(3)–O(3)	176.4(13)
P(2)–Re(2)–C(5)	91.4(4)	Re(2)–C(4)–O(4)	177.7(14)
P(2)–Re(2)–C(6)	93.8(5)	Re(2)–C(5)–O(5)	176.5(11)
O(7)–Re(2)–O(8)	74.8(3)	Re(2)–C(6)–O(6)	176.8(15)
O(7)–Re(2)–C(4)	96.4(6)	P(1)–C(9)–P(2)	116.3(6)
O(7)–Re(2)–C(5)	170.1(4)		
Dihedral Angles			
Re(1)–Re(2)–P(2)–P(1) = Re(2)–Re(1)–P(1)–P(2)			2.3(1)
O(7)–Re(1)–Re(2)–O(8)			12.3(5)
Re(1)–O(7)–O(8)–Re(2)			9.4(3)

73 atoms, 406 parameters, and 2056 out of 2407 reflections and converged with  $R_F = 0.021$ ,  $R' = 0.024$  (for all reflections,  $R = 0.036$  and  $R' = 0.025$ ). The goodness of fit is 1.04. Weights based on counting statistics were used. The weight modifier was 0.000 100. The maximum shift/error ratio was 0.006. In the last difference map the deepest hole was  $-0.310 \text{ e } \text{Å}^{-3}$ , and the highest peak  $0.470 \text{ e } \text{Å}^{-3}$ . Computations were carried out on a Microvax 3600 computer with the NRCC package. Final atomic coordinates and selected bond distances and angles are listed in Tables 2 and 3, respectively.

**Acknowledgment.** We acknowledge the National University of Singapore (NUS) (Grant No. RP850030) for financial support and technical assistance from the Department of Chemistry, NUS. Scholarship awards from NUS to P.M.N.L. and Y.K.Y. are acknowledged.

We appreciate assistance from Y. P. Leong in the preparation of this paper.

## Appendix

In dynamic laser-light scattering (DLS), the intensity–intensity time correlation function  $G^{(2)}(t)$  in the self-beating mode is measured which has the form

$$G^{(2)}(t) = A[1 + \beta|g^{(1)}(t)|^2]$$

where  $A$  is a measured base line;  $\beta$  is a parameter depending on the coherence of the detection,  $t$  is the delay time, and  $g^{(1)}(t)$ , the normalized first-order electric field time correlation function. In general,  $g^{(1)}(t)$  is related to the line width distribution  $G(\Gamma)$  by

$$g^{(1)}(t) = \int G(\Gamma)e^{-\Gamma t} d\Gamma$$

$G(\Gamma)$  can be calculated from the measured  $G^{(2)}(t)$  by a Laplace inversion. For a diffusive relaxation,  $\Gamma$  is further related to the translational diffusion coefficient  $D$  of the particle by

$$\Gamma = Dq^2$$

where

$$q = (4\pi n/\lambda_0) \sin(\theta/2)$$

is the scattering vector with  $n$ ,  $\lambda_0$ , and  $\theta$  being the refractive index of the solvent, the light wavelength, and the scattering angle, respectively.

$D$  can be further converted to the hydrodynamic radius  $(1/R_h)^{-1}$ , or simply  $R_h$ , by the Stokes–Einstein equation:

$$D = k_B T/6\pi\eta R_h$$

In this equation,  $k_B$  is the Boltzmann constant,  $T$  is the absolute temperature, and  $\eta$  is the solvent viscosity. Therefore,  $G(\Gamma)$  can be converted into a hydrodynamic radius distribution  $f_z(R_h)$ . The subscript  $z$  indicates that this distribution is an intensity distribution. This can then be further converted to the weight distribution  $f_w(R_h)$ , where  $f_w(R_h) = \{f_z(R_h)/R_h^3\}/\sum\{f_z(R_h)/R_h^3\}$ .

**Supporting Information Available:** Details of the X-ray structural analysis for  $[\text{Re}_2(\mu\text{-Ome})_2(\mu\text{-dppm})(\text{CO})_6]$ , including tables of crystallographic data, refined atomic coordinates and isotropic thermal parameters, anisotropic thermal parameters, bond distances and angles, and torsion angles (10 pages). Ordering information is given on any current masthead page. Listings of structure factors (9 pages) can be obtained from L.-K.L.

OM9506779